Stochastic Variability of Tropical Cyclone Intensity at the Asymptotic Potential Intensity Equilibrium

Phuong Nguyen[1]

[1]Department of Mathematics,Texas Tech University, Lubbock, TX 79409

Chanh Kieu[2] *

[2]Department of Earth and Atmospheric Sciences, Indiana University, Bloomington, IN 47405.

Wai Tong Fan[3]

[3]Department of Mathematics, Indiana University, Bloomington, IN 47405

**Corresponding author address:* Chanh Kieu. Department of Earth and Atmospheric Sciences, Indiana University, Bloomington, IN 47405

E-mail: ckieu@indiana.edu

ABSTRACT

This study examines the variability of tropical cyclone (TC) intensity associated with stochastic forcings at the maximum potential intensity (PI) equilibrium. By representing TC intensity in terms of the Wiener process in the framework of TC-scale dynamics, it is shown that there exists an invariant intensity distribution whose variance is proportional to and roughly half of the variances of stochastic forcings. This result advocates recent findings that TC dynamics possesses an intrinsic variability, which prevents the TC absolute intensity errors in numerical models from being reduced below an arbitrarily small threshold. Analysis of the invariant intensity distribution at the PI limit reveals further that the stochastic forcing component associated with tangential wind and warm core anomaly in the TC central region have the largest effects on TC intensity variability. These results suggest that future development of stochastic parameterization in TC model should focus on representation of both tangential wind and thermodynamic structure to capture proper TC intensity fluctuations.

1. Introduction

Stochastic processes are a natural property of all atmospheric systems. These random variabilities exist in various spatial and temporal scales, and are often related to unknown fluctuations in physical systems, especially at micro and turbulent scales (Hasselmann 1976; Palmer 2001; Penland 2003; Williams et al. 2016; Berner et al. 2017). Accounting for these stochastic processes in numerical weather prediction models is challenging either at resolved or unresolved model resolutions, due to our inadequate understanding of different physical components as well as nonlinear interaction at different scales (Palmer 2001; Penland 2003; Tompkins and Berner 2008; Weisheimer et al. 2014). In practice, the atmospheric randomness is commonly accounted for in numerical models via an ensemble representation of stochastic physics, in which physical parameterization schemes employ a random variation of model parameters or add random variations to model variables to mimic uncertainties in the atmosphere (Palmer 2001; Christensen et al. 2015; Dorrestijn et al. 2015).

Given such a stochastic nature of the atmosphere, a fundamental question that has not been fully examined in the tropical cyclone (TC) research is how much of intensity errors in real-time TC forecasts are caused by stochastic forcings. This question is of significance to the current effort in improving the accuracy of TC intensity forecasts in numerical models, because it dictates the degree of intensity variability associated with random processes that we could never fully control. With the current 4-5 day intensity errors in operational TC models around 11-18 kt (Tallapragada et al. 2014, 2015; Bhatia and Nolan 2015; Emanuel and Zhang 2016; Kieu et al. 2018), determining how much of these TC intensity errors are related to stochastic forcings will provide some additional information about our maximum ability in reducing TC intensity errors that we can achieve in the future.

Similar to any atmospheric system, TC intensity forecast errors in numerical models are generally due to several factors such as the intrinsic nature of TC intensity variability, model errors, imperfect initial conditions, or random factors (see, e.g., Tallapragada et al. 2014; Jin et al. 2014; Tallapragada et al. 2015; Zhang et al. 2015; Penny et al. 2016; Doyle et al. 2017; Halperin and Torn 2018; Kieu et al. 2018). It is difficult, if at all impossible, to isolate the relative contribution of these error sources in practice due to their nonlinear interaction once models are integrated. Using the TC-scale dynamics framework, Kieu and Moon (2016); Kieu et al. (2018) recently proposed that a substantial part of TC intensity errors in numerical models is related to the existence of a chaotic attractor at the TC maximum potential intensity (PI) limit. Even in an idealized environment with a perfect dynamical model, the chaotic behavior of TC dynamics can be responsible for an intrinsic intensity fluctuation with a variance in the range of 6-8 ms^{-1} in the absence of any random processes. This result has a significant implication for operational TC forecasting, because it reveals internal characteristics of TC dynamics that prevent us from knowing precisely TC intensity at any given time, regardless of how accurate the observing systems or how perfect TC models are.

Despite such insights about chaotic behaviors of TC intensity derived from the TC-scale framework, the deterministic chaos at the PI limit as proposed by Kieu and Moon (2016) is based only on the axisymmetrical dynamics of Rotunno and Emanuel (1987)'s model. While this full-physics model could provide detailed processes of TC dynamics and thermodynamics, the use of a numerical model to solve the TC governing equations immediately introduces new difficulties in quantifying the intrinsic TC intensity variability. Specifically, various numerical truncation errors and filtering schemes are implemented in the model to eliminate numerical noises and maintain the model numerical stability. Thus, the same model configuration and initial/boundary condition could lead to different realization of atmospheric states when running on different machines or compilation/libraries. These completely numerical artifacts produce very similar behaviors to models with stochastic forcings in the sense that the same model and initial condition result in different model outcomes. In this regard, it is natural to consider any TC model as a stochastic rather than a deterministic dynamical system. [1].

As a result of this stochastic nature of TC models, the estimation of the size of the chaotic PI attractor presented in Kieu and Moon (2016) contains unknown contribution from stochastic processes that are in addition to the TC intrinsic dynamics. Hence, a very natural, yet open, question is *how much of TC intensity variability at the PI limit is caused by stochastic forcings as compared to the chaotic variability*. This question is significant because of the fundamental difference between chaotic and stochastic variability. That is, one could have a dynamical system whose state fluctuation in the phase space is completely chaotic without any stochastic forcings, and vice versa.

Among different approaches to tackle the above question, the most compelling way is to use a numerical model with stochastic physics parameterizations so one can examine how TC intensity fluctuation changes when varying stochastic forcing amplitudes. Sampling an ensemble of outputs from these stochastic model simulations would then allow one to quantify TC intensity variability as a function of forcing variances. Although this stochastic ensemble approach appears to be promising and is indeed applied in current operational forecasting centers for TC applications (see, e.g. Zhang et al. 2015), the myriad of degrees of freedom in current numerical models makes it virtually impossible to isolate what stochastic components are most relevant for TC intensity variability. For example, there is no specific guidance on how to add random perturbations to temperature, moisture, model parameters, or wind variables. Likewise, one can arbitrarily add

[1] Strictly speaking, a stochastic dynamics contains a collection of random variables indexed by time, which could lead to different trajectories due to different realization of the random forcings when running the same model.

random noises to upper levels, low levels, at the surface, or any part of the model domain. Such a large degree of freedom in implementing the stochastic forcing in full-physics TC models results in an infinite number of possibilities, which may not be helpful to understand TC intensity variability associated with stochastic processes.

Recent studies by Kieu (2015); Kieu and Wang (2017, 2018) suggest a pathway to probe the problem of TC intensity fluctuation caused by stochastic forcing. Using TC scales as dynamical variables, they presented a fidelity-reduced model that could capture several fundamental aspects of TC development such as the PI equilibrium and stability, the consistency of the wind-induced surface heat exchange mechanism and the PI equilibrium, or an inherent timescale for TC rapid intensification. A particular feature of this TC-scale model is its explicit time-dependence with only 3 degrees of freedom, which correspond to the maximum tangential wind, the maximum radial wind, and the warm core anomaly at the TC center. The explicit time-dependence of this TC-scale model allows a transparent way to investigate the effects of stochastic forcings that are most relevant to TC dynamics in the absence of deterministic chaos. Furthermore, one can also quantify the relative importance of dynamical stochastic forcing versus thermodynamic stochastic forcing in TC development, which could not be obtained directly from full-physics simulations.

Given the usefulness of the TC-scale dynamics model, two specific questions related to TC intensity stochastic fluctuations that we wish to present in this study are 1) how much of TC intensity variability can be induced by stochastic forcings at the PI limit, and 2) what stochastic forcing component plays the most important role in TC intensity fluctuations. These questions are of practical, as they provide more insight into the mechanisms that prevent us from reducing TC intensity errors below a certain threshold beyond the deterministic chaos. Moreover, knowing the relative role of different stochastic forcing components will allow us to properly design stochastic ensemble forecasting for future TC intensity forecast applications.

The structure of the paper is organized as follows. In the next section, a brief introduction of the TC-scale model and its extension for a stochastic system will be presented. Section 3 derives some theoretical estimations of the probability density at the PI limit, and Section 4 presents numerical analyses of the Monte-Carlo integration of the stochastic TC-scale model. Some concluding remarks are summarized in the final section.

2. Formulation

a. TC-scale model

Using scale analyses for the TC governing equations, Kieu and Wang (2017, 2018) obtained the following set of nondimensionalized equations for TC scales under the wind-induced surface heat exchange (WISHE) feedback parameterization:

$$\begin{cases} \dot{u} = pv^2 - (p+1)b - uv \\ \dot{v} = -uv - v^2 \\ \dot{b} = bu + su + v - rb \end{cases} \tag{1}$$

where (u, v, b) denote the non-dimensional scales of the maximum surface radial wind, the maximum surface tangential wind and the temperature anomaly in the eye region respectively; p is a constant proportional to the squared ratio of the depth of the troposphere to the depth of the boundary layer, s denotes the effective tropospheric static stability, and r represents the Newtonian cooling. Details derivations of this TC-scale system can be found in Kieu and Wang (2017).

Despite its simplicity, the TC-scale model (1) contains several important proprieties. First, this system possesses a unique stable point $(1, 1, 1)$ in the phase space of (u, v, b) that corresponds exactly to Emanuel's PI solution under the strict moist neutrality condition (i.e., $s = 0$). This is a non-trivial result, as the derivation of the PI solution from the TC-scale dynamics is very different from the previous approaches based on the energy cycle or the gradient wind balance (Emanuel 1986, 1988). Second, this system could demonstrate that the WISHE feedback is dynamically consistent with the PI equilibrium, a result that has largely been demonstrated by numerical simulations but not rigorously proven. Third, the PI equilibrium derived from the above TC-scale model indicates that this equilibrium must be simultaneously constrained by three variables (u, v, b), rather than just the value of the maximum tangential wind v as in the classical PI theory (Emanuel 1986, 1988). For example, a TC vortex with the maximum tangential wind that is exactly equal to the PI value (i.e., $v = 1$), but a too weak or a too strong warm core (i.e., $b < 1$ or $b > 1$) would lead immediately to a strong fluctuation of TC intensity with time before settling in the PI equilibrium. Last, the TC-scale model suggests two different time scales for TC development; a shorter timescale is related to the oscillation of TCs around the gradient wind balance state, and a longer timescale is associated with rapid intensification of the TC vortex toward a balance between the frictional forcing and the absolute angular momentum convergence. More detailed discussions of these results can be found in Kieu (2015); Kieu and Wang (2017, 2018).

b. A stochastic extension

While the TC-scale model of Eq. (1) is appealing and is able to capture several key features of TC dynamics, this deterministic model does not contain any stochastic components that exist in real physical systems. As such, we examine in this study a stochastic extension of Eq. (1) to address a specific question related to TC intensity fluctuation caused by stochastic forcings. Our main aim is to quantify the asymptotic probability distribution of TC intensity variability with different stochastic variances, and then determine which component of the stochastic forcings has the largest impact on TC intensity fluctuations at the PI limit.

For this purpose, we consider a TC-scale stochastic model in which the random forcings are represented by three independent Wiener processes $\mathbf{W}_t = (W_t^1, W_t^2, W_t^3)$. Specifically, the extended TC-scale model is given as follows:

$$d\mathbf{X}_t = \mathbf{F}(\mathbf{X}_t)\,dt + \sigma\,d\mathbf{W}_t\ , \tag{2}$$

where $\mathbf{X}_t \equiv (u,v,b)$ denotes a vector of continuous-time Markov processes in the phase space of (u,v,b), $\mathbf{F} \equiv (f_1, f_2, f_3) \equiv (pv^2 - (p+1)b - uv, -uv - v^2, bu + su + v - rb)$ are deterministic forcings of the TC-scale model as given in Eq. (1), and σ a constant 3×3 diagonal matrix that characterizes the magnitude and covariance among three stochastic forcing components.

Our first aim is to analyze the long time behavior of Eq. (2) such that the variance of the TC intensity distribution can be quantified in terms of the model parameters as well as the stochastic forcing matrix σ. Before deriving several important properties of the intensity distribution, we recall a well-known theorem that Eq. (2) has a unique solution $\mathbf{X}$, since the function $\mathbf{F}$ is locally Lipschitz. This solution represents a diffusion process with an invariant measure $\mu_X(\vec{x})$ that satisfies the stationary Fokker-Planck equation [2]

$$\sum_{i=1}^{3} \frac{\sigma_i^2}{2} \frac{\partial^2 \mu_X(\vec{x})}{\partial x_i^2} - \sum_{i=1}^{3} \frac{\partial (f_i(\vec{x})\mu_X(\vec{x}))}{\partial x_i} = 0 \tag{3}$$

where $\vec{x} = (x_1, x_2, x_3) = (u,v,b)$ and $(f_1, f_2, f_3) \equiv (pv^2 - (p+1)b - uv, -uv - v^2, bu + su + v - rb)$ defined in the half space $\mathbb{R} \times \mathbb{R}_+ \times \mathbb{R}$ (i.e. cyclonic wind $v \geq 0$), along with the Dirichlet boundary condition.

Introducing a normalizing constant $C = \int_{\mathbb{R}\times\mathbb{R}_+\times\mathbb{R}} \mu_X < \infty$, the marginal distribution of the v-component in μ_X will then have a probability density given by

$$\mu_{X,2}(x) = \frac{1}{C} \int_{\mathbb{R}} \int_{\mathbb{R}} \mu_X(x_1, x, x_3)\,dx_1\,dx_3, \quad x \geq 0. \tag{4}$$

[2] Mathematically, the invariant distribution can be precisely defined as $\int \mathscr{L} f(x)\mu(dx) = 0$ for all f in the domain of the infinitesimal generator $\mathscr{L}$ associated with (2).

Thus, the desired mean and variance of the v-component in μ_X are

$$\bar{v} = \int_{\mathbb{R}} x\,\mu_{X,2}(x)\,dx, \quad \sigma_v = \int_{\mathbb{R}} x^2\,\mu_{X,2}(x)\,dx - \bar{v}^2. \tag{5}$$

While it is not known whether and how fast the solution to Eq. (2) converges to μ_X, assessing the stationary intensity distribution in terms of model parameters could at least help answer a central question of how much of TC intensity variability inside the PI chaotic attractor proposed in Kieu and Moon (2016) is related to stochastic forcings as mentioned in the Introduction. In the next section, we will derive a few key asymptotic properties of Eq. (2) at the PI equilibrium under some specific approximations. Full numerical integration of Eq. (2) and related analyses will be followed in Section 5.

3. Stochastic framework

In order to make sense of the stochastic term in (2), we first recall some definitions and some properties of real-valued Brownian motion or Wiener process and stochastic processes.

Definition 3.1 *A σ - algebra is a collection $\mathscr{U}$ of subsets of Ω with these properties*

i. $\emptyset, \omega \in \mathscr{U}$

ii. If $A \in \mathscr{U}$ then $A^c \in \mathscr{U}$.

iii. If $A_1, A_2, ... \in \mathscr{U}$, then

$$\cap_{k=1}^{\infty} A_k \in \mathscr{U}, \ \cup_{k=1}^{\infty} A_k \in \mathscr{U}$$

Here, $A^c := \Omega - A$ is the complement of A.

Definition 3.2 *Let $\mathscr{U}$ be a-algebra of subsets of Ω. We call $\mathbb{P} : \mathscr{U} \to [0,1]$ probability measure provided:*

i. $\mathbb{P}(\emptyset) = 0, \qquad \mathbb{P}(\Omega) = 1.$

- *If* $A_1, A_2, \ldots$ *are disjoint sets in* $\mathscr{U}$ *, then*

$$\mathbb{P}(\cup_{k=1}^{\infty} A_k) = \sum_{k=1}^{\infty} \mathbb{P}(A_k)$$

Definition 3.3 *A triple* $(\Omega, \mathscr{U}, \mathbb{P})$ *is called a probability space provided* Ω *is any set,* $\mathscr{U}$ *is a* σ*-algebra, and* $\mathbb{P}$ *is a probability measure on* $\mathscr{U}$*.*

Definition 3.4 *Let* $(\Omega, \mathscr{U}, \mathbb{P})$ *be a probability space. A mapping*

$$\mathbf{X} : \Omega \to \mathbb{R}^n$$

is called an n-dimensional random variable if for each $B \in \mathscr{B}$*, we have*

$$\mathbf{X}^{-1}(B) = \{\omega : \mathbf{X}(\omega) \in B\} \in \mathscr{U}$$

where $\mathscr{B}$ denotes the collection of Borel subsets of $\mathbb{R}^n$, which is the smallest σ- algebra of subsets of $\mathbb{R}^n$ containing all open sets.

Definition 3.5 *(Stochastic processes)*

i. A collection $\{\mathbf{X}(t) | t \geq 0\}$ *of random variables is called a stochastic process.*

ii. For each point $\omega \in \Omega$*, the mapping* $t \to \mathbf{X}(t, \omega)$ *is the corresponding sample path.*

Definition 3.6 *We call*

$$\mathbb{E}(\mathbf{X}) = \int_{\Omega} \mathbf{X} d\mathbb{P}$$

the expected value (or mean value) of $\mathbf{X}$*.*

Definition 3.7 *We call*

$$\mathbb{V}(\mathbf{X}) = \int_{\Omega} |\mathbf{X} - \mathbb{E}\mathbf{X}|^2 d\mathbb{P}$$

the variance of $\mathbf{X}$*.*

Let $(\Omega, \mathscr{U}, \mathbb{P})$ be a probability space and let $\mathbf{X} : \Omega \to \mathbb{R}^n$

Definition 3.8 *(Distribution functions)*

i. The distribution function of $\mathbf{X}$ *is the function* $F_{\mathbf{X}} : \mathbb{R}^n \to [0,1]$ *defined by*

$$F_{\mathbf{X}}(x) := \mathbb{P}(\mathbf{X} \leq x), \forall x \in \mathbb{R}^n$$

ii. If $\mathbf{X}_1, ..., \mathbf{X}_m : \Omega \to \mathbb{R}^n$ *are random variables, then joint distribution function is*

$$F_{\mathbf{X}_1,...,\mathbf{X}_m}(x_1, ..., x_m) := \mathbb{P}(\mathbf{X_1} \leq x_1, ..., \mathbf{X_m} \leq x_m), \qquad \forall x_i \in \mathbb{R}^n,\ i = 1, 2, ..., m.$$

Definition 3.9 *Suppose* $\mathbf{X} : \Omega \to \mathbb{R}^n$ *is a random variable and* $F = F_{\mathbf{X}}$ *its distribution. If there exists a nonnegative, integrable function* $f : \mathbb{R}^n \to \mathbb{R}$ *such that*

$$F(x) = F(x_1, ..., x_n) = \int_{-\infty}^{x_1} ... \int_{-\infty}^{x_n} f(y_1, ..., y_m) dy_n ... dy_1,$$

then f *is called the density function for* $\mathbf{X}$.

Example 3.1 *If* $f : \Omega \to \mathbb{R}$ *has density*

$$f(x) = \frac{1}{\sqrt{2\pi\sigma^2}} e^{\frac{-|x-m|^2}{2\sigma^2}}, \qquad x \in \mathbb{R},$$

we say $\mathbf{X}$ *has a Gaussian(or normal) distribution, with mean m and variance* σ^2*. In this case, let us write* $\mathbf{X}$ *is an* $\mathscr{N}(m, \sigma^2)$ *random variable or Gaussian random variable.*

Example 3.2 *If* $f : \Omega \to \mathbb{R}^n$ *has density*

$$f(x) = \frac{1}{\sqrt{(2\pi)^n detC}} e^{\frac{-1(x-m).C^{-1}.(x-m)}{2}} \qquad (x \in \mathbb{R}^n)$$

for some $m \in \mathbb{R}^n$ *and some positive definite, symmetric matrix C, we say* $\mathbf{X}$ *has a Gaussian (or normal) distribution, with mean m and covariance matrix C. We then write* $\mathbf{X}$ *is an* $\mathscr{N}(m, C)$ *random variable.*

Definition 3.10 *A real-valued stochastic process $W(\cdot)$ is called a Brownian motion or Wiener process if*

i. $W(0) = 0$ *a.s.,*

ii. $W(t) - W(s)$ *is* $\mathcal{N}(0, t-s)$ *for all* $t \geq s \geq 0$

iii. *For all time* $0 < t_1 < t_2 \ldots < t_n$*, the random variable* $W(t_1), W(t_2) - W(t_1), \ldots, W(t_n) - W(t_{n-1})$ *are independent.*

Theorem 3.1 *(Itô's formula) Suppose that $X(\cdot)$ has a stochastic differential*

$$dX = F dt + G dW$$

Assume $u : \mathbb{R} \times [0, T] \to \mathbb{R}$ is continuous and that $\frac{\partial u}{\partial t}, \frac{\partial u}{\partial x}, \frac{\partial^2 u}{\partial x^2}$ exist and are continuous. Then the process $Y = u(X(t), t)$ satisfies the stochastic differential

$$dY = \left(\frac{\partial u}{\partial t} + \frac{\partial u}{\partial x} F + \frac{1}{2} \frac{\partial^2 u}{\partial x^2} G^2 \right) dt + \frac{\partial u}{\partial x} G dW$$

Theorem 3.2 *(Itô product rule) Suppose*

$$\begin{cases} dX_1 = F_1 dt + G_1 dW \\ dX_2 = F_2 dt + G_2 dW \end{cases} \tag{6}$$

Then,

$$d(X_1 X_2) = X_2 dX_1 + X_1 dX_2 + G_1 G_2 dt.$$

4. Invariant intensity distribution

A traditional approach to the problem of determining the probability density in a stochastic differential equation is to construct a Fokker-Planck equation for the given equation, and then solve this Fokker-Planck equation to obtain the probability density (see, e.g. Durrett 2010; Ø ksendal

2003). Once the probability density function is known, the asymptotic behaviors can be explicitly found by taking the limit $t \to \infty$ (i.e., by explicitly solving equation (3)) as discussed in the previous section. While the full time-dependent Fokker-Plank equation for the stochastic TC-scale model (2) can be easily constructed, it is virtually impossible to solve this equation due to the nonlinear terms in Eq (2). Furthermore, the particular deterministic forcing terms f_i in Eq. (2) does not ensure the positive or negative definiteness for all points in the phase space. As such, analytical approach for this Fokker-Plank equation will not be pursued here.

The existence of a unique asymptotically stable point of the TC-scale model in the absence of random processes presented in Kieu and Wang (2017) suggests however a different pathway to this problem. Since we are more concerned with the variability only near the stable point, it is possible to study the intensity distribution by linearizing the stochastic TC-scale model around the PI equilibrium, assuming that the stochastic forcings are sufficiently small that do not create new equilibria in the phase space of (u, v, b). This assumption is strongly supported by numerical analyses of the TC-scale model in Kieu (2015); Kieu and Wang (2017), which showed that the PI equilibrium in the TC-scale dynamics is extremely resilient to any perturbation. Regardless of initial TC intensity and model parameters, the TC-scale dynamics will always converge to a single point in the phase space due to the strong balance between frictional forcing and absolute angular momentum convergence. Provided that the elements of the stochastic forcing matrix σ are not too large, we will hereinafter assume that the PI equilibrium in the TC-scale model also exists, even with the stochastic extension as will be verified by numerical analyses in Section 4,

With the above consideration, we study now a linearized Eq. (2) around a critical stable point $\mathbf{x}_c$ of the TC-scale model, which is given by $\mathbf{x}_c \equiv (-\sqrt{1-s}, \sqrt{1-s}, (1-s))$ in the absence of the radiative cooling (i.e., $r = 0$). This critical point can be shown to correspond to the PI limit as discussed in Kieu (2015). Note that the main effect of radiative cooling in the TC-scale model is to introduce a trapping region near the origin $(0,0,0)$ in the phase space of (u,v,b) with little change to the PI equilibrium. In full-physics model simulations, many previous studies have also confirm the minor role of the radiative cooling to the PI limit (see also Rotunno and Emanuel1987, Wing et al. 2020). Thus, we will simplify our analysis in this study by focusing on the PI equilibrium such that radiative cooling impacts on the stability as well as the value of the PI limit can be neglected.

Let $\mathbf{A} = (a_{ij})_{i,j=1}^{3}$ be the Jacobian matrix of the TC-scale model at the critical point $\mathbf{x}_c$ and shift the origin of the TC-scale model to $\mathbf{x}_c$ as $\mathbf{X} = \mathbf{Y} + \mathbf{x}_c$, it is readily then to obtain the following linearized system for the perturbation variable $\mathbf{Y}$

$$d\mathbf{Y}_t = A\,\mathbf{Y}_t\,dt + \sigma\,d\mathbf{W}_t \tag{7}$$

where $\mathbf{W}_t$ is the standard three-dimensional Brownian motion, and $\mathbf{A}$ is given by (see Eq. (35) Kieu and Wang 2017).

$$\mathbf{A} = \begin{pmatrix} -\sqrt{1-s} & (2p+1)\sqrt{1-s} & -p-1 \\ -\sqrt{1-s} & \sqrt{1-s} & 0 \\ 1 & 1 & \sqrt{1-s} \end{pmatrix}, \tag{8}$$

Note that a stochastic solution $\mathbf{X}$ to the original Eq. (2) will not necessarily stay near $\mathbf{x}_c$ (corresponding to cyclonic wind $v > 0$), but in principle can visit any other potential stable critical point $\mathbf{x}_c$ once stochastic forcings included. However, given our above assumption of the unique stable PI attractor, it is expected that the stationary intensity distribution of $\mathbf{Y}$ will be close to that of $\mathbf{X}$ around the equilibrium $\mathbf{x}_c$. Thus, $\mathbf{Y} + \mathbf{x}_c$ is a good approximation to $\mathbf{X}$ when $\mathbf{X}$ is sufficiently close to $\mathbf{x}_c$. For the sake of terminology, we will hereinafter define an *invariant intensity distribution* (a.k.a. *stationary distribution*) of $\mathbf{Y}_t$ as a probability measure μ_Y such that if $\mathbf{Y}_0 \sim \mu_Y$, then $\mathbf{Y}_t \sim \mu_Y$ for all $t \geq 0$.

Note that for the special case when $\mathbf{A}$ is symmetric and negative definite, the invariant distribution μ_Y is a multivariate normal distribution (the Gaussian distribution) with a mean $\mathbf{0} \in R^3$ and the co-variance matrix is just the inverse of the product $-\frac{1}{2}\sigma A^{-1}\sigma^T$, as shown in Appendix 1. For the TC-scale model, we note however that $\mathbf{A}$ is not symmetric as shown in Eq. (8). Therefore, the negative definiteness is not ensured, even when the solution $\mathbf{Y}_t$ approaches the stable point $\mathbf{0}$. This asymptotic convergence is related to the property of the TC-scale dynamics, which possesses a simple Lyapunov stability instead of uniformly asymptotic stability at $\mathbf{0}$ [3]. Because of the unknown definiteness of $\mathbf{A}$, we will seek an invariant intensity distribution for the strong solution Y_t to Eq. (7) indirectly. Indeed, apply Itô's Lemma to the function $F(t, \mathbf{Y}_t) = e^{-t\mathbf{A}}\mathbf{Y}_t$, the (strong) solution $\mathbf{Y}_t$ to Eq. (7) is then obtained formally as

$$\mathbf{Y}_t = e^{t\mathbf{A}}\mathbf{Y}_0 + \int_0^t e^{(t-s)\mathbf{A}}\sigma \cdot d\mathbf{W}_s, \quad t \geq 0. \tag{9}$$

Note that $\int_0^t e^{(t-s)A}\sigma \cdot d\mathbf{W}_s$ is a centered Gaussian random variable with a co-variance matrix

$$\rho(t) = \int_0^t e^{(t-s)\mathbf{A}}\sigma\,(e^{(t-s)\mathbf{A}}\sigma)^T\,ds = \int_0^t e^{(t-s)\mathbf{A}}\sigma\sigma^T\,e^{(t-s)\mathbf{A}^T}\,ds = \int_0^t e^{s\mathbf{A}}\sigma\sigma^T\,e^{s\mathbf{A}^T}\,ds, \tag{10}$$

which converges, as $t \to \infty$, to a 3 by 3 matrix

$$\rho_Y = \int_0^\infty e^{s\mathbf{A}}\sigma\sigma^T\,e^{s\mathbf{A}^T}\,ds. \tag{11}$$

Under the assumption of the Lyapunov stability of the TC-scale dynamics, the strong solution $\mathbf{Y}_t$ to Eq. (7) exists for all time and has a unique invariant distribution μ_Y, which is a centered Gaussian random variable $\mathcal{N}(\mathbf{0}, \rho_Y)$ with a co-variance matrix ρ_Y. Furthermore, since $\mathbf{A}$ possesses 3 distinct eigenvalues $\{\lambda_i\}_{i=1}^3$ that all have negative real parts,$\mathbf{Y}_t$ converges in distribution to μ_Y exponentially fast as $t \to \infty$.

---

[3]The subtlety between two types of the stability can be directly seen using the linearized equation $\mathbf{x}^T\frac{d\mathbf{x}}{dt} = \frac{1}{2}\frac{d(\mathbf{x}^T\mathbf{x})}{dt} = \mathbf{x}^T\mathbf{A}\mathbf{x}$. Apparently, it is possible that $\frac{d(\mathbf{x}^T\mathbf{x})}{dt} > 0$ for some time t_0, even when $\lim_{t\to\infty}\mathbf{x}(t) = e^{\mathbf{A}t} \to \mathbf{0}$. So, the negative definite property of $\mathbf{A}$ is not conclusive.

To find the covariance matrix ρ_Y explicitly without the complication of integrating the matrix exponent in Eq. (11), one can look for a more direct approach that determines the time dependence of the covariance matrix $\rho(t) \equiv \mathbb{E}[\mathbf{Y}_t \mathbf{Y}_t^*]$ at each time t. Indeed, applying the Itô product formula to the function $\varphi(t,\omega) = \mathbf{Y}(t)\mathbf{Y}^*(t)$, we obtain

$$d(\mathbf{Y}(t)\mathbf{Y}^*(t)) = \mathbf{Y}d\mathbf{Y}^* + \mathbf{Y}^*d\mathbf{Y} + \sigma\sigma^* dt$$

We then apply the expected value to each side and note that A is a non-random matrix and $\mathbb{E}(YdW_t) = \mathbb{E}(Y^*dW_t) = 0$

$$\mathbb{E}d(\mathbf{Y}(t)\mathbf{Y}^*(t)) = d(\mathbb{E}(\mathbf{Y}(t)\mathbf{Y}^*(t)) = d\rho = \mathbb{E}\Bigg([(d\mathbf{Y})\mathbf{Y}^*] + [\mathbf{Y}d\mathbf{Y}^*)] + [(\sigma\sigma^*)dt] \Bigg) \tag{12}$$

$$= \mathbb{E}\Bigg(\mathbf{Y}^*A\mathbf{Y}dt + \sigma\mathbf{Y}^*dW_t + \mathbf{Y}A\mathbf{Y}^*dt + \sigma^*\mathbf{Y}dW_t + \sigma\sigma^*dt \Bigg) \tag{13}$$

$$= \mathbb{E}[\mathbf{A}\mathbf{Y}\mathbf{Y}^*dt] + \mathbb{E}[\mathbf{Y}\mathbf{Y}^*\mathbf{A}^*dt] + \sigma\sigma^*dt \tag{14}$$

$$= \mathbf{A}\mathbb{E}[\mathbf{Y}\mathbf{Y}^*]dt + E[\mathbf{Y}\mathbf{Y}^*]\mathbf{A}^*dt + \sigma\sigma^*dt \tag{15}$$

$$= \Bigg[(\mathbf{A}\rho + \rho\mathbf{A}^*) + \sigma\sigma^*\Bigg]dt \tag{16}$$

Thus, the matrix differential equation for the covariance density $\rho(t)$ is given as follows

$$\dot{\rho} = \mathbf{A}\rho + \rho\mathbf{A}^* + \sigma\sigma^* \tag{17}$$

The covariance matrix ρ_Y of the invariant density in Eq. (11) can be then obtained by setting $\dot{\rho} = 0$ in Eq. (17) to yield:

$$\mathbf{A}\rho_{\mathbf{Y}} + \rho_{\mathbf{Y}}\mathbf{A}^* + \sigma\sigma^* = 0 \tag{18}$$

As can be seen from either Eq. (11) or Eq. (18), the calculation of the invariant distribution μ_Y requires an explicit expression for the stochastic forcing matrix σ. Although it is difficult to solve Eq. (18) for a general case in which stochastic forcings are strongly correlated (i.e.,$\sigma_{ij} \neq 0, i \neq j$), the calculation will be much simplified when σ is a diagonal matrix $\sigma = diag(\sigma_1, \sigma_2, \sigma_3)$.

That is, the stochastic forcing components are uncorrelated to each other such that $\sigma\sigma^T = \sigma^2$. Physically, this assumption of a diagonal stochastic forcing matrix σ means than stochastic forcing components in the TC-scale model are independent for different variables, which is reasonable in the real atmosphere due to the isotropic property of randomness.

Under this assumption of uncorrelated stochastic forcings, one can derive a formal expression for the covariance matrix ρ_Y in terms of eigenvalues and eigenvectors of $\mathbf{A}$. Indeed, applying the Schur decomposition $\mathbf{A} = \mathbf{QDQ}^*$, where $\mathbf{D}$ is an upper triangular matrix with eigenvalues on its diagonal and $\mathbf{Q}$ is Hermitian matrix satisfying $\mathbf{QQ}^* = \mathbf{I}$, we have

$$\mathbf{QDQ}^*\rho_Y + \rho_Y\mathbf{QD}^*\mathbf{Q}^* = -\sigma\sigma^* \tag{19}$$

Multiplying Eq. (19) by $\mathbf{Q}^*$ from the left and $\mathbf{Q}$ from the right and defining $\bar{\rho} = \mathbf{Q}^*\rho_\mathbf{Y}\mathbf{Q}$, and $\bar{L} = -\mathbf{Q}^*\sigma\sigma^*\mathbf{Q}$, the co-variance matrix ρ_Y then satisfies the following general Sylvester equation

$$\mathbf{D}\bar{\rho} + \bar{\rho}\mathbf{D}^* = \bar{L} \tag{20}$$

Therefore, the procedure to find the invariant distribution matrix ρ_Y essentially consists of three basic steps: 1) applying the Schur decomposition to matrix $\mathbf{A}$ to obtain $\mathbf{D}$ and $\mathbf{Q}$, 2) solving the Sylvester equation (20) for $\bar{\rho}$, and 3) inverting the relationship $\bar{\rho} = \mathbf{Q}^*\rho_\mathbf{Y}\mathbf{Q}$ to obtain ρ_Y. Note that $\mathbf{D}$ and $\mathbf{D}^*$ are the upper and lower triangle matrices, respectively. As such, one can solve Eq. (20) for each entry $\bar{\rho}_{ij}$ at a time, using the back substitution once the diagonal entries of the left and the right hand side of (20) are solved first (see Appendix 3 for the formal solution to Eq. (20)).

Without all the details of solving the Sylvester equation, we list here several important remarks from the derivations of the invariant intensity distribution. First, the above computation of the invariant distribution based on (20) requires explicit knowledge of the unknown matrices $\mathbf{Q}$ and $\mathbf{D}$ as well as all eigenvalues. Assuming general values of the Jacobian matrix $\mathbf{Q}, \mathbf{D}$, Appendix 3 shows a detailed derivation of all elements of $\bar{\rho}$. Even under this most general form of the matrices $\mathbf{Q}, \mathbf{D}$, one can see clearly the linear dependence of $r\bar{h}o$ on the variances of the stochastic forcing matrix σ, and inverse dependence on the eigenvalues of $\mathbf{A}$. Of course, the closed form for $\bar{\rho}_{ij}$ requires explicit expressions of $\mathbf{A}$ and its eigenvalues, which are computationally difficult to derive. However, the formal integral invariant distribution given by Eq. (11) or the solution to Eq. (20) is still important, because it shows that an invariant Gaussian distribution exists and how to obtain it. Second, due to our asymptotic approach, the exponential decay of the tail distribution is not known from either the close integral form or the stationary limit of $\dot{\rho} = 0$. This question must be therefore verified by using a numerical approach that we will present in the next section. Last, the above analysis should, in principle, work for any dimension, and so it can be also extended to other types of stochastic forcings such as non-diagonal or degenerate matrix σ if necessary.

5. Numerical analyses

a. Invariant density of TC intensity variability

In this section, we will use a numerical approach to verify and provide additional details into the analyses presented in Section 3. Specifically, we wish to extract the variance of the v-wind component σ_v defined in (5), which is also contained in the general covariance intensity matrix (11), given the variances $\sigma_1^2, \sigma_2^2, \sigma_3^2$. This v-variance is practically meaningful, because it represents the variability of TC intensity that forecasters most concern from the operational perspective. In addition to extract σ_v, it is necessary to confirm also the exponential decay of the tail distribution of TC intensity towards an invariant distribution at the PI limit as assumed in Section 3. Unlike the analytical derivations that are linearized around the maximum potential intensity critical point, direct numerical integration of Eq. (2) allows for addressing the above questions explicitly in the full nonlinear form.

To have a broad picture of full nonlinear behaviors of the stochastic TC-scale model (2), we consider a set of parameters shown in Table 1, which are typical for TCs under a real atmospheric environment (see Kieu 2015; Kieu and Wang 2017). By default, Eqs. (2) are numerically integrated for 10000 time steps, using the standard Runge-Kutta fourth-order scheme with a time step $dt = 0.001$ (in nondimensional unit) similar to that in Kieu and Wang (2017). Due to the random nature of the stochastic forcings, the Monte-Carlo ensemble method is employed in all experiments, with 1000 different realizations of the model integration for each set of parameters and initial condition.

Among several model parameters, we note specifically in our numerical experiments that the standard deviations $\sigma_1, \sigma_2, \sigma_3$ of the stochastic forcings in Eq. (2) are set to be the same with values of $(0.01, 0.01, 0.01)$ to ease our comparison with the analytical solution presented in Section 3. These nondimensional amplitudes correspond to a random forcing variation of $\sim 0.2\ ms^{-1}$ per hour for the (u, v) components, and $\sim 0.003\ m^2s^{-2}$ per hour for the buoyancy variable in the physical space (i.e., a random variation of $\sim 0.5\ K$ per hour in terms of potential temperature). Such variations are well within the typical random fluctuations of atmospheric wind speed, which are the same in both the radial and tangential directions, and the temperature in the central region of real TCs (see, e.g., French et al. 2007; Zhang 2010).

As an illustration, Figure 1 shows one specific realization of the numerical integration, starting from four arbitrary initial conditions in the phase space of (u, v, b) One notices in Figure 1 that consistent with our assumption of the existence of a unique attractor in the phase space of (u, v, b), all trajectories of Eq. (2) converges quickly towards the PI attractor, even with the stochastic forcing included. Provided that the variances of stochastic forcings are smaller than 0.3 (in nondimensional unit), this attractor behavior is very robust, regardless of initial conditions. For any value of σ_1, σ_2 or σ_3 larger than 0.3, the system (2) however becomes unstable and develops a wind field with random negative values (i.e., an anticyclonic flow). As a result, the TC-scale model (1) will immediately blow up due to the emergence of an unstable critical point in the anticyclonic domain with $v < 0$ (see Kieu 2015; Kieu and Wang 2017). The existence of such a unique stable attractor in the stochastic TC-scale model is important, because it verifies our assumption of the convergence of the model flows towards an intensity invariant distribution ρ_Y, as examined in Section 3.

Along with the existence of a stable region in the phase space with an invariant intensity distribution ρ_Y, one can see apparently from Figure 1 that the orbits are now no longer smooth curves as in the original deterministic system. Instead, the flows are strongly fluctuated as they approach the attractor in the phase space, rather than a single unique stable point. In this regard, the invariant intensity distribution ρ_Y as given by (11) can be seen as the bounded region in the phase space in which TC intensity variation is most likely located as expected.

We should particularly emphasize at this point that while an invariant density distribution of a stochastic system differs from a chaotic attractor of a deterministic system, it is practically impossible to distinguish the variability of TC intensity within the invariant density distribution from that inside the chaotic attractor. One could in principle wait for a sufficient long time such that a large fluctuation of TC intensity associated with the invariant probability distribution could be realized, which helps indicate if the attractor is chaotic or stochastic. However, for all real TC development, TCs may not have much time to stay at the PI limit before weakening due to landfalling or moving to higher latitudes. Therefore, the fluctuation of TC intensity in real TC development could be a manifestation of both TC chaotic dynamics and the stochastic nature of atmosphere that one cannot fully separate.

To help quantify the characteristics of the invariant intensity distribution at the PI equilibrium, Figure 2 shows the projection of the flow orbits onto the v direction for the three orbits shown in Figure 1. The random effects are clearly manifested in this time series, with a rapid fluctuation of TC intensity during the entire TC development very similar to the actual TC intensity observed from high temporal resolution aircraft observation (French et al. 2007; Zhang 2010). Of more interest is the fluctuation of TC intensity at the asymptotic limit $t \to \infty$, which represents the invariant intensity distribution μ_Y examined in Section 3. For the control experiments with $\sigma_1 = \sigma_2 = \sigma_3 = 0.01$, the corresponding standard derivation of the TC intensity variation in the v direction σ_v is ~ 0.0056, which is less than 1% of the typical PI value. For example, if one assumes a PI value of 65 $m\,s^{-1}$ and a time scale of 3 hours as given in Table 3, the fluctuation of TC intensity at the PI limit due to the stochastic forcing is only ~ 0.4 $m\,s^{-1}$, which is relatively small compared to the typical TC intensity errors in real-time forecasts (see, e.g. Tallapragada et al. 2014; Kieu and Moon 2016; Kieu et al. 2018).

Because of the dependence of μ_Y on the amplitudes of stochastic forcings, Figure 3 shows the standard derivation σ_v for TC intensity at the asymptotic limit $t \to \infty$ for a range of $\sigma_1 = \sigma_2 = \sigma_3 \in [0.01 - 0.1]$. Despite the nonlinear behavior of the stochastic TC-scale model (2), one notices in Figure 3 that σ_v varies almost linearly with σ_i and is roughly half of the standard derivation σ_i. Such a linear dependence of σ_v on the variance of the stochastic forcing σ_i is consistent with the analytical derivation in Section 3 (see also Appendix 3). Indeed, if one applies $\sigma_1 = \sigma_2 = \sigma_3 = \sigma_f$ to the Sylvester equation (20), the explicit solution (see Appendix 3) to this equation will give σ_v that is linearly proportional to the variance of the stochastic forcing, i.e., $\sigma_v^2 \sim \sigma_f^2$ as expected. The numerical simulations in this regard confirm the asymptotic analyses presented in the previous section.

As a way to further examine the derivation of the asymptotic invariant intensity distribution ρ_Y as given by Eq (11), we note that the linear dependence of σ_v on the stochastic forcing variance σ_i is realized not only for the special case $\sigma_1 = \sigma_2 = \sigma_3$ but also for each individual variance of stochastic forcing (i.e., $\sigma_i \neq 0$, but $\sigma_{j,k} = 0, i \neq j \neq k$) as can be directly seen in the explicit expression of σ_v shown in Appendix 3.

To verify this property, Figure 4 shows the standard derivation σ_v for a range of the stochastic forcing variance. That is, only one σ_i is varied, while setting the other two variances $\sigma_j, j \neq i$ equal to zero. As shown in Figure 4, the TC intensity variance σ_v indeed increases linearly with each σ_i as expected from the linearized analyses. Among the three variances of the stochastic forcings, it is of interest to note however that σ_v is most sensitive to the tangential wind forcing (i.e., σ_2) and the temperature forcing (i.e., σ_3), while it is much less sensitive to the radial wind forcing (i.e., σ_1 as seen from the scale of the y-axis in Figure 4). This result has some significant implication, because it indicates that the fluctuation in tangential wind v or the temperature anomaly b will have far more reaching impacts on TC intensity variability. Therefore, future effort of optimizing a TC vortex initialization should focus more on the tangential wind and temperature structure than on the secondary circulation for operational purposes.

From the physical perspective, an important question for the above numerical results is whether or not the assumptions for the stochastic matrix σ are reasonable. While the numerical results obtained in this section and the analytical derivations in Section 3 confirm the importance of stochastic forcings in TC intensity fluctuation during TC development as well as at the PI limit, one notices that stochastic intensity fluctuation shown in Figure 3 is significantly less than the variability due to the deterministic chaos or real-time intensity errors found in Kieu and Moon (2016); Kieu et al. (2018). Only for a stochastic forcing standard derivation as larger as 2 ms^{-1} per hour does the standard derivation of TC intensity variation reach roughly 4 ms^{-1}, which is still smaller than 8 $m\,s^{-1}$ as obtained from the axisymmetric simulations in Kieu and Moon (2016) or real-time intensity errors Tallapragada et al. (2013, 2014); Kieu et al. (2018). Such a smaller value of TC intensity variability that is induced by random processes indicates that the existence of the deterministic PI chaotic attractor is indeed needed to fully account for the observed intensity variation.

On the other hand, the fact that TC intensity can vary with a standard deviation as large as $4ms^{-1}$ at the PI limit due to random forcing reiterates that the absolute intensity errors in a numerical model, especially for models with a stochastic parameterization scheme such as the Hurricane Weather Research and Forecasting model (Zhang et al. 2015), will have an intrinsic barrier of 4 $m\,s^{-1}$ that one cannot reduce further. The combination of the stochastic variations as found in this study and the potential existence of a chaotic PI attractor as found in Kieu and Moon (2016); Kieu et al. (2018) thus imposes a very strong upper bound on the accuracy of TC dynamical models in the future, if the metric for TC intensity is based on the maximum 10-m wind.

b. Stochastic nonlinear versus linear effects

Although the numerical integration of the stochastic TC-scale model could capture an invariant probability distribution of TC intensity that supports the linearized analyses at the PI limit, an important question that has not been examined so far is whether the invariant density μ_X from the nonlinear model (2) accords with μ_Y obtained from the linearized model (7). In addition, it is also necessary to examine if the dependence of the invariant intensity density on the model parameters is consistent between these nonlinear and the linearized models. By varying the two model parameters p and s and comparing the variances of the TC intensity distribution obtained from the linearized and the full nonlinear models, it is possible to assess the nonlinear effects on TC intensity density that we wish to explore in this subsection.

In this regard, Figure 5 shows the variances of TC intensity distributions from Eqs. (2) and (7) when one of the model key parameters p or s is varied while all other parameters are fixed. Recall here that these two parameters encode significant amount of TC dynamics; s represents the degree of slantwise moist neutrality, and p is the squared ratio of the boundary layer depth over the tropospheric depth that is scaled by the drag coefficient. Unlike the linearized model whose invariant density can be derived explicitly, note that numerical integrations of the full nonlinear stochastic systems require a large number of experiments to capture as many realizations of random forcings as possible.

One notices in Figure 5 that the nonlinear and linear models display an overall a consistent functional dependence on the model parameters. Specifically, both models capture an invariant density that increases with a larger parameter s shown in Figure 5a). Likewise, both models show an inverse relationship between the variance of intensity distribution and the model parameter p (Fig. 5b). Physically, these results indicates that a more stable troposphere would produce a higher intensity variability, given the same magnitude of random forcings. This is because a more stable atmosphere would allow a weaker PI limit, thus resulting a stronger fluctuation of TC intensity similar to a stochastic fluctuation inside a lower potential well. On the other hand, a higher value of p means weaker boundary layer frictional forcing, which tends to attain a higher PI limit that confines more the intensity fluctuation inside. Thus, a smaller intensity variance for a larger value of p is expected.

Within the statistical significance level of the numerical simulations, one notices however that the nonlinear and linear models do not completely comparable in terms of the value of intensity variance. In fact, full nonlinear model captures a higher intensity variance for a range of parameters p and s. The two models are only comparable when the effective static stability parameter s is sufficiently high (> 0.6), or the aspect ratio p is sufficiently small (< 300). Beyond these ranges, the nonlinear model tends to capture a higher intensity variance than that obtained from the linearized model at the PI limit. In this regard, the above result could highlight the regime in the parameter space where the invariant density distribution derived from the linearized model is acceptable for analytical purposes.

6. Conclusion

In this study, a low-order stochastic model based on TC scales was presented to study the asymptotic probability density of TC intensity at the PI equilibrium. By introducing stochastic forcings to the TC-scale model in the form of Wiener processes, a number of important findings related to the asymptotic properties of TC intensity variability have been obtained. First, it was shown that there exists an invariant intensity distribution at the PI equilibrium whose variance is linearly proportional to the variance of stochastic forcings. That is, the larger the stochastic forcing variance, the more TC intensity fluctuation one would expect at the PI limit. Second, our analytical and numerical analyses showed that the standard deviation of this probability intensity distribution is roughly half of the standard derivation of the stochastic forcings in the nondimensionalized space. In the full dimensional form, this result indicates that a stochastic forcing with a wind speed variation of 1-2 ms^{-1} per hour or temperature variation of 1-2 K per hour could lead to an intensity variation of $\sim 3-4ms^{-1}$.

Third, among different stochastic forcing components, the stochastic forcings related to tangential wind and the temperature anomaly at TC central region have the largest impact on TC intensity variation, whereas stochastic forcing in the radial direction has a much smaller effect. The dominant role of tangential wind and warm core anomaly forcings advocate that future TC model development should focus more on improving an initial representation of tangential wind and TC thermodynamic structure to optimize TC intensity forecast accuracy.

From the practical standpoint, these results are non-trivial because they suggest an inherent limit in the absolute TC intensity errors that one cannot reduce further in operational TC models where random factors can never be eliminated. As long as the maximum 10-m wind is used as a metric to measure TC intensity, the absolute TC intensity forecast errors will have a barrier at which one cannot reduce further. We note that this limit in our capability to reduce TC intensity errors below a certain threshold associated with stochastic forcings fundamentally differs from that due to chaotic dynamics; the invariant density has an unbounded density distribution that could accept a probability of having an arbitrarily high intensity, whereas the chaotic dynamics has a strictly bounded attractor. For all practical purposes, the chaotic and stochastic intensity fluctuations are however not separable. They both contribute to TC intensity variability that prevents one from reducing TC intensity errors below a certain threshold.

While the stochastic TC-scale model presented in this study could demonstrate the fluctuation of TC intensity associated with random forcing, a number of caveats must be acknowledged. First, the randomness introduced in this TC-scale framework is somewhat different from the true randomness in real atmosphere. This is because real atmosphere possesses some coherent structure whose random variables may not be completely uncorrelated as assumed in this study (i.e., the stochastic forcing matrix ■ may not be diagonal). For analytical analyses, this correlated stochastic forcings results in such a complicated form of density matrix that there may exist no explicit form for the invariant density, even at the PI asymptotic limit. Second, the TC-scale dynamics used in this study is drastically simplified as compared to the dynamics of real TCs for which various subtle physical and thermodynamic processes are essential. Thus, the intensity variation obtained in this simplified TC-scale model cannot capture nonlinear interactions among different physical components of real TCs, thus resulting in some uncertainties in quantifying the intensity fluctuation related to stochastic forcings. In this regard, TC intensity variation due to stochastic forcings examined in this study can serve only as a lower bound for the actual intensity fluctuations in real TCs.

Acknowledgments. This research was supported by the ONR Young Investigator Program (Award NA16NWS4680026). CK wishes to thank the NCAR/ASP visiting program for their summer support and hospitality during the preparation of this work.

APPENDIX

Appendix 1

For the case of a symmetric Jacobian matrix A, we can re-write the linearized equation in terms of the gradient form as follows:

$$d\mathbf{Y}_t = \nabla\Phi(\mathbf{Y}_t)\,dt + \Sigma\,d\mathbf{W}_t, \tag{A1}$$

where $\Phi(\mathbf{x}) = \frac{1}{2}\mathbf{x}^T A\mathbf{x} = \frac{1}{2}\sum_{i,j=1}^{3} a_{ij}x_i x_j$. Define the matrix

$$\widetilde{A} = 2(\Sigma^{-1})^2 A = \left(\frac{2\,a_{ij}}{\sigma_i^2}\right)_{i,j}.$$

Suppose $\sigma_i \neq 0$ for all $i \in \{1,2,3\}$ and A is symmetric. Then the (strong) solution Y to (7) is a symmetric diffusion with symmetrization measure $e^{\widetilde{\Phi}(\mathbf{x})}\,d\mathbf{x}$, where

$$\widetilde{\Phi}(\mathbf{x}) = \frac{1}{2}\mathbf{x}^T\widetilde{A}\mathbf{x} = \frac{1}{2}\sum_{i,j=1}^{3}\frac{2\,a_{ij}}{\sigma_i^2}x_i x_j.$$

Furthermore, if $Z := \int_{\mathbb{R}^3}\exp\widetilde{\Phi}(\mathbf{x})\,d\mathbf{x} < \infty$, then Y has a unique invariant measure

$$\mu_Y(d\mathbf{x}) = \frac{e^{\widetilde{\Phi}(\mathbf{x})}\,d\mathbf{x}}{Z}.$$

In particular, if $\widetilde{A}$ is symmetric, then μ_Y is the multivariate normal distribution (the Gaussian distribution) with mean $\mathbf{0} \in R^3$ and co-variance matrix

$$-\begin{pmatrix} 2a_{11}/\sigma_1^2 & 2a_{12}/\sigma_1^2 & 2a_{13}/\sigma_1^2 \\ 2a_{21}/\sigma_2^2 & 2a_{22}/\sigma_2^2 & 2a_{23}/\sigma_2^2 \\ 2a_{31}/\sigma_3^2 & 2a_{32}/\sigma_3^2 & 2a_{33}/\sigma_3^2 \end{pmatrix}^{-1} = -\frac{1}{2}A^{-1}\Sigma^2.$$

The condition $Z := \int_{\mathbb{R}^3}\exp\widetilde{\Phi}(\mathbf{x})\,d\mathbf{x} < \infty$ is satisfied if A is negative definite in the sense that $\mathbf{x}^T A\mathbf{x} < 0$ for all nonzero $\mathbf{x}$.

(Sketch) The generator of the solution Y is

$$\begin{aligned}\mathscr{L}f(\mathbf{x}) =&\frac{1}{2}\sum_{i=1}^{3}\sigma_i^2\frac{\partial^2 f}{\partial x_i^2}(\mathbf{x})+\nabla\Phi\cdot\nabla f(\mathbf{x})\\ =&\frac{1}{2}\sum_{i=1}^{3}\sigma_i^2\frac{\partial^2 f}{\partial x_i^2}(\mathbf{x})+\sum_{i=1}^{3}\left(\sum_{j=1}^{3}a_{ij}x_j\right)\frac{\partial f}{\partial x_i}(\mathbf{x})\\ =&\frac{1}{2}\sum_{i=1}^{3}\sigma_i^2\left\{\frac{\partial^2 f}{\partial x_i^2}(\mathbf{x})+\left(\sum_{j=1}^{3}\frac{2a_{ij}}{\sigma_i^2}x_j\right)\frac{\partial f}{\partial x_i}(\mathbf{x})\right\}\\ =&\frac{1}{2\rho(\mathbf{x})}\sum_{i=1}^{3}\frac{\partial\left(\rho(\mathbf{x})\,\sigma_i^2\,\frac{\partial f}{\partial x_i}(\mathbf{x})\right)}{\partial x_i}\end{aligned}$$

where $\rho(\mathbf{x})=e^{\widetilde{\Phi}(\mathbf{x})}$.

The condition $Z:=\int_{\mathbb{R}^3}\exp\widetilde{\Phi}(\mathbf{x})\,d\mathbf{x}<\infty$ is satisfied if A is negative definite, because $\widetilde{A}$ is negative definite if and only if A is negative definite. To see the last statement, observe that $\widetilde{A}=DA$ where $D=2(\Sigma^{-1})^2$ is a diagonal matrix with positive entries. Hence for each $k\in\{1,2,3\}$, the determinant of the upper left k by k sub-matrix of $\widetilde{A}$ has the same sign as that for A.

Appendix 2

The eigenvalues of the Jacobian matrix (38) in Kieu and Wang (2017) have negative real parts, so the critical point is stable in the ODE system (30)-(32) in that paper. In this Appendix, we investigate how the absolute values of the real parts of the eigenvalues control the rate of convergence of the SDE (7) towards its invariant distribution μ_Y.

(L^2-Exponential convergence) Let X be a Markov process with stationary measure μ. Let $\{P_t\}_{t\geq 0}$ be the semigroup of X. We say that L^2 exponential ergodicity holds for X if there exists $c\in(0,\infty)$ such that

$$\left\|P_t f-\int f\,d\mu\right\|_{L^2(\mu)}\leq e^{-ct}\left\|f-\int f d\mu\right\|_{L^2(\mu)} \tag{A2}$$

for all $f\in\mathscr{C}_b(\mathscr{S})$ and $t\geq 0$. This means the probability distribution of X_t converges to the stationary distribution exponentially fast. It is well known (van Handel 2014, Chapter 2) that for reversible ergodic Markov processes with a positive spectral gap, L^2 exponential ergodicity (A2) holds. This implies that (A2) holds for our multi-dimensional Ornstein–Uhlenbeck process Y, since all eigenvalues of A have negative real parts.

Appendix 3. Formal solution for the covariance matrix ρ_Y

To solve the Sylvester equation formally, let

$$\mathbf{Q} = \begin{pmatrix} \alpha_1 & \alpha_2 & \alpha_3 \\ \beta_1 & \beta_2 & \beta_3 \\ \delta_1 & \delta_2 & \delta_3 \end{pmatrix}$$

and

$$\bar{\rho} = \begin{pmatrix} \bar{\rho}_{11} & \bar{\rho}_{12} & \bar{\rho}_{13} \\ \bar{\rho}_{21} & \bar{\rho}_{22} & \bar{\rho}_{23} \\ \bar{\rho}_{31} & \bar{\rho}_{32} & \bar{\rho}_{33} \end{pmatrix}$$

and

$$\mathbf{D} = \begin{pmatrix} \lambda_1 & a_1 & a_2 \\ 0 & \lambda_2 & a_3 \\ 0 & 0 & \lambda_3 \end{pmatrix}$$

We compute

$$\bar{L} = Q^* \sigma \sigma^* Q = \begin{pmatrix} \bar{L}_{11} & \bar{L}_{12} & \bar{L}_{13} \\ \bar{L}_{21} & \bar{L}_{22} & \bar{L}_{23} \\ \bar{L}_{31} & \bar{L}_{32} & \bar{L}_{33} \end{pmatrix}$$

where

- $\bar{L}_{11} = -(\alpha_1^2\sigma_1^2 + \beta_1^2\sigma_2^2 + \delta_1^2\sigma_3^2)$
- $\bar{L}_{12} = -(\alpha_1\alpha_2\sigma_1^2 + \beta_1\beta_2\sigma_2^2 + \delta_1\delta_2\sigma_3^2)$
- $\bar{L}_{13} = -(\alpha_1\alpha_3\sigma_1^2 + \beta_1\beta_3\sigma_2^2 + \delta_1\delta_3\sigma_3^2)$

- $\bar{L}_{21} = \alpha_1\alpha_2\sigma_1^2 + \beta_1\beta_2\sigma_2^2 + \delta_1\delta_2\sigma_3^2$

- $\bar{L}_{22} = -(\alpha_2^2\sigma_1^2 + \beta_2^2\sigma_2^2 + \delta_2^2\sigma_3^2)$

- $\bar{L}_{23} = -(\alpha_2\alpha_3\sigma_1^2 + \beta_2\beta_3\sigma_2^2 + \delta_2\delta_3\sigma_3^2)$

- $\bar{L}_{31} = -(\alpha_1\alpha_3\sigma_1^2 + \beta_1\beta_3\sigma_2^2 + \delta_1\delta_3\sigma_3^2)$

- $\bar{L}_{32} = -(\alpha_2\alpha_3\sigma_1^2 + \beta_2\beta_3\sigma_2^2 + \delta_2\delta_3\sigma_3^2)$

- $\bar{L}_{33} = -(\alpha_3^2\sigma_1^2 + \beta_3^2\sigma_2^2 + \delta_3^2\sigma_3^2)$

By using the back substitution, we are able to derive the solution for the system (**??**) as follows

$$\bar{\rho}_{33} = \frac{\bar{L}_{33}}{2Re(\lambda_3)}, \qquad \bar{\rho}_{32} = \frac{\bar{L}_{32} - \bar{a}_3\bar{\rho}_{33}}{\lambda_3 + \bar{\lambda}_2},$$
$$\bar{\rho}_{31} = \frac{\bar{L}_{31} - \bar{a}_1\bar{\rho}_{32} - \bar{a}_2\bar{\rho}_{33}}{\lambda_3 + \bar{\lambda}_1}, \qquad \bar{\rho}_{23} = \frac{\bar{L}_{23} - \bar{a}_3\bar{\rho}_{33} - \bar{\lambda}_2\bar{\rho}_{23}}{\lambda_2}$$
$$\bar{\rho}_{22} = \frac{\bar{L}_{22} - \bar{a}_3\bar{\rho}_{32} - \bar{a}_3\bar{\rho}_{23}}{2Re(\lambda_2)}, \qquad \bar{\rho}_{21} = \frac{\bar{L}_{21} - a_3\bar{\rho}_{31} - \bar{a}_2\bar{\rho}_{23} - \bar{a}_1\bar{\rho}_{22}}{\bar{\lambda}_1 + \lambda_2}$$
$$\bar{\rho}_{13} = \frac{\bar{L}_{13} - a_1\bar{\rho}_{23} - a_2\bar{\rho}_{33}}{\lambda_1 + \bar{\lambda}_3}, \qquad \bar{\rho}_{12} = \frac{\bar{L}_{12} - a_1\bar{\rho}_{22} - a_2\bar{\rho}_{32} - \bar{a}_3\bar{\rho}_{13}}{\lambda_1 + \bar{\lambda}_2}$$
$$\bar{\rho}_{11} = \frac{\bar{L}_{11} - a_1\bar{\rho}_{21} - a_2\bar{\rho}_{31} - \bar{a}_1\bar{\rho}_{12} - \bar{a}_2\bar{\rho}_{13}}{2Re(\lambda_1)} \quad \text{(A3)}$$

By utilizing the relation $\bar{\rho} = \mathbf{Q}^*\rho_{\mathbf{Y}}\mathbf{Q}$, all entries of the co-variance matrix ρ_Y are found explicitly.

References

Berner, J., and Coauthors, 2017: Stochastic parameterization: Toward a new view of weather and climate models. *Bull. Amer. Meteor. Soc.*, **98**, 565–588.

Bhatia, K. T., and D. S. Nolan, 2015: Prediction of Intensity Model Error (PRIME) for Atlantic Basin Tropical Cyclones. *Wea. Forecasting*, **30 (6)**, 1845–1865, doi:10.1175/WAF-D-15-0064.1, URL http://journals.ametsoc.org/doi/abs/10.1175/WAF-D-15-0064.1.

Budhiraja, A., and W. Fan, 2017: Uniform in time interating particle approximations for nonlinear equations of keller-segel type. *Electronic Journal of Probability*, **22**.

Christensen, H., I. Moroz, and T. Palmer, 2015: Stochastic and perturbed parameter representations of model uncertainty in convection parameterization. *J. Atmos. Sci.*, **72**, 2525–2544.

Dorrestijn, J., D. Crommelin, H. J. A.P. Siebesma, and C. Jakob, 2015: Stochastic parameterization of convective area fractions with a multicloud model inferred from observational data. *J. Atmos. Sci.*, **72**, 854–869.

Doyle, J. D., and Coauthors, 2017: A view of tropical cyclones from above: The tropical cyclone intensity experiment. *Bulletin of the American Meteorological Society*, **98 (10)**, 2113–2134, doi:10.1175/BAMS-D-16-0055.1.

Durrett, R., 2010: *Probability: theory and examples*, Cambridge Series in Statistical and Probabilistic Mathematics, Vol. 31. 4th ed., Cambridge University Press, Cambridge, x+428 pp., URL https://doi.org/10.1017/CBO9780511779398.

Emanuel, K. A., 1986: An air-sea interaction theory for tropical cyclones. part i: Steady-state maintenance. *J. Atmos. Sci.*, **43**, 585–605.

Emanuel, K. A., and F. Zhang, 2016: On the Predictability and Error Sources of Tropical Cyclone Intensity Forecasts. *J. Atmos. Sci.*, **73 (9)**, 3739–3747, doi:10.1175/JAS-D-16-0100.1, URL http://journals.ametsoc.org/doi/full/10.1175/JAS-D-16-0100.1.

French, J., W. Drennan, J. Zhang, and P. Black, 2007: Turbulent fluxes in the hurricane boundary layer. part i: Momentum flux. *J. Atmos. Sci*, **64**, 1089–1102.

Halperin, D. J., and R. D. Torn, 2018: Diagnosing conditions associated with large intensity forecast errors in the hurricane weather research and forecasting (hwrf) model. *Weather and Forecasting*, **33 (1)**, 239–266, doi:10.1175/WAF-D-17-0077.1.

Hasselmann, K., 1976: Stochastic climate models. part i: Theory. *Tellus*, **28**, 473–485.

Jin, Y., and Coauthors, 2014: The impact of ice phase cloud parameterizations on tropical cyclone prediction. *Monthly Weather Review*, **142 (2)**, 606–625, doi:10.1175/MWR-D-13-00058.1.

Kieu, C., K. Keshavamurthy, V. Tallapragada, S. Gopalakrishnan, and S. Trahan, 2018: On the growth of intensity forecast errors in the operational hurricane weather research and forecasting (hwrf) model. *Q. J. R. Meteorol. Soc.*, **144**, 1803–1819.

Kieu, C. Q., 2015: Hurricane maximum potential intensity equilibrium. *Q.J.R. Meteorol. Soc.*, **141 (692)**, 2471–2480, doi:10.1002/qj.2556.

Kieu, C. Q., and Z. Moon, 2016: Hurricane Intensity Predictability. *Bull. Amer. Meteor. Soc.*, doi:10.1175/BAMS-D-15-00168.1.

Kieu, C. Q., and Q. Wang, 2017: Stability of tropical cyclone equilibrium. *J. Atmos. Sci.*, **74**, 3591–3608.

Kieu, C. Q., and Q. Wang, 2018: On the scale dynamics of the tropical cyclone intensity. *Discrete and Continuous Dynamical Systems - B*, **23**, 3047.

Ø ksendal, B., 2003: *Stochastic differential equations*. Sixth ed., Universitext, Springer-Verlag, Berlin, xxiv+360 pp., URL https://doi.org/10.1007/978-3-642-14394-6, an introduction with applications.

Palmer, T. N., 2001: A nonlinear dynamical perspective on model error: A proposal for non-local stochastic–dynamic parametrization in weather and climate prediction models. *Quart. J. Roy. Meteor. Soc*, **127**, 279–304.

Penland, C., 2003: Noise out of chaos and why it won't go away. *Bull. Amer. Meteor. Soc*, **84**, 921–925.

Penny, A. B., P. A. Harr, and J. D. Doyle, 2016: Sensitivity to the representation of microphysical processes in numerical simulations during tropical storm formation. *Monthly Weather Review*, **144 (10)**, 3611–3630, doi:10.1175/MWR-D-15-0259.1.

Tallapragada, V., C. Kieu, Y. Kwon, S. Trahan, Q. Liu, Z. Zhang, and I.-H. Kwon, 2014: Evaluation of Storm Structure from the Operational HWRF during 2012 Implementation. *Mon. Wea. Rev.*, **142**, 4308–4325, doi:10.1175/MWR-D-13-00010.1.

Tallapragada, V., and Coauthors, 2013: Hurricane Weather Research and Forecasting (HWRF) model: 2013 scientific documentation. *Developmental Testbed Center*, **99**.

Tallapragada, V., and Coauthors, 2015: Forecasting Tropical Cyclones in the Western North Pacific Basin using the NCEP Operational HWRF Model. Model Upgrades and Evaluation of Real-Time Performance in 2013. *Wea. Forecasting*, doi:10.1175/WAF-D-14-00139.1.

Tompkins, A. M., and J. Berner, 2008: A stochastic convective approach to account for model uncertainty due to unresolved humidity variability. *J. Geophys. Res.*, **113**, D18 101.

van Handel, R., 2014: Probability in high dimension. Tech. rep., PRINCETON UNIV NJ.

Weisheimer, A., S. Corti, T. N. Palmer, and . F. Vitart, 2014: Addressing model error through atmospheric stochastic physical parametrizations: Impact on the coupled ecmwf seasonal forecasting system. *Philos. Trans. Roy. Soc. London*, 2013029.

Williams, P., N. Howe, J. Gregory, R. Smith, and M. Joshi, 2016: Improved climate simulations through a stochastic parameterization of ocean eddies. *J. Climate*, **29**, 8763–8781.

Wing, A. A., J. Ruppert, X. Tang, and E. L. Duran, 2020: The importance of radiative feedbacks in tropical cyclogenesis. *Tropical Meteorology and Tropical Cyclones Symposium*, **3.4**, URL https://ams.confex.com/ams/2020Annual/meetingapp.cgi/Paper/364527.

Zhang, J., 2010: Estimation of dissipative heating using low-level in situ aircraft observations in the hurricane boundary layer. *J. Atmos. Sci*, **67**, 1853–1862.

Zhang, Z., V. Tallapragada, C. Kieu, S. Trahan, and W. Wang, 2015: Hwrf based ensemble prediction system using perturbations from gefs and stochastic convective trigger function. *Tropical Cyclone Research and Review*, **3**, 145–161.

LIST OF TABLES

TABLE 1. Default values of all parameters in the stochastic TC-scale model that are used for the numerical integration of Eq. (2)

Parameter	Value	Remark
V_c	$\sim 65ms^{-1}$	Scale of the maximum surface wind at the PI equilibrium for sea surface temperature of 30^oC.
U_c	$\sim 10ms^{-1}$	Scale of the radial wind at the PI equilibrium.
B_c	$\sim 0.4ms^{-2}$	Scale of the maximum buoyancy that corresponds to the warm core in the TC eye region
T	$\sim 10^4s$	A characteristic time scale
p	200	nondimensional square ratio of the PBL depth over the radius of the maximum wind
r	0.1	a nondimensional parameter representing the radiative cooling
s	0.1	a nondimensional parameter representing the tropospheric stratification
σ_1	0.01	nondimensional variance of the u-wind stochastic forcing component
σ_2	0.01	nondimensional variance of the v-wind stochastic forcing component
σ_3	0.01	nondimensional variance of the buoyancy stochastic forcing component

LIST OF FIGURES

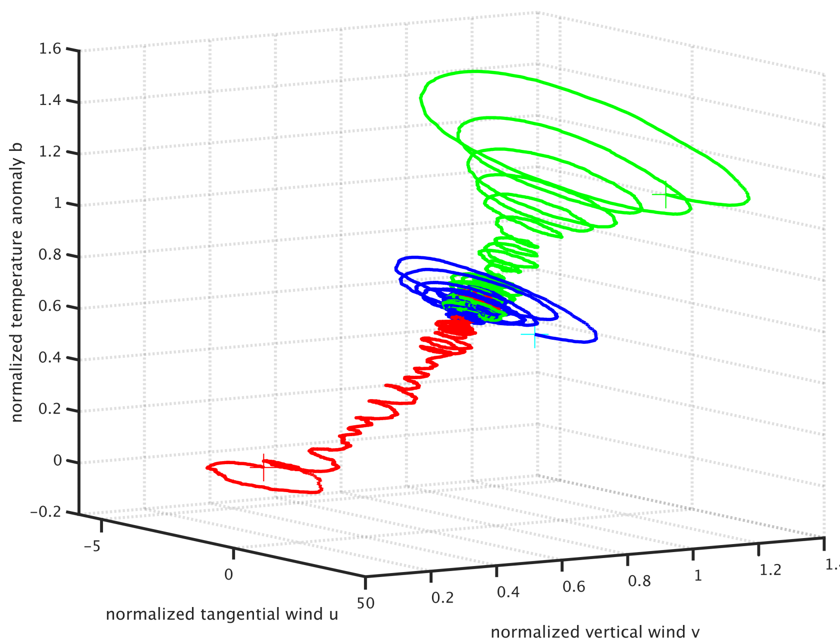

676 FIG. 1. Orbits of the flow in the stochastic TC-scale model for three different initial conditions that are
677 obtained from the numerical integration of Eq. (2), assuming the parameter given in Table 1.

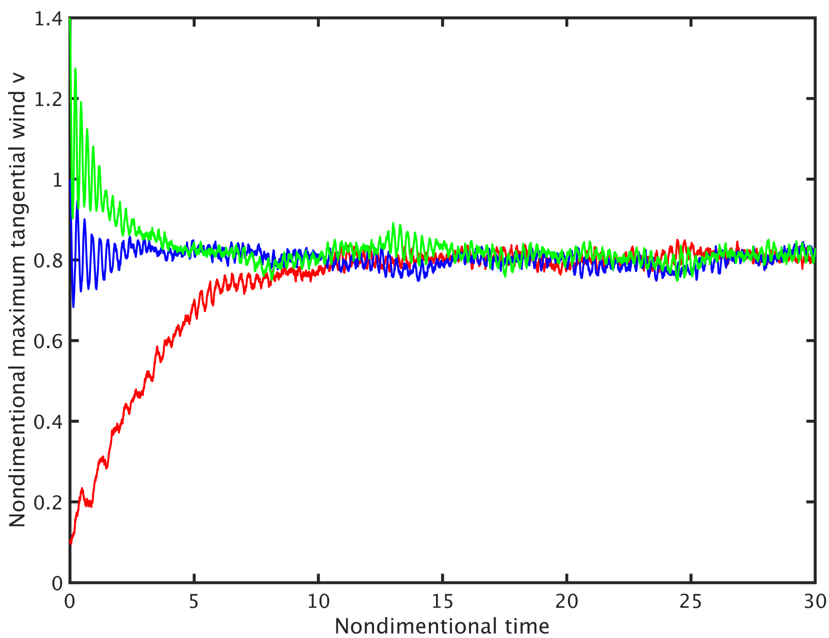

FIG. 2. Time series of the v component for the three orbits shown in Figure 1.

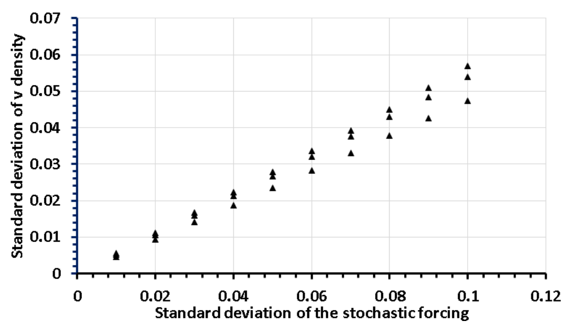

FIG. 3. Dependence of the standard deviation of the TC intensity (i.e., the v component) of the invariant intensity distribution ρ_Y as given by Eq. (11) of the stochastic TC-scale model on the standard deviation $\sigma_1 = \sigma_2 = \sigma_3$ of the stochastic forcing at the PI limit.

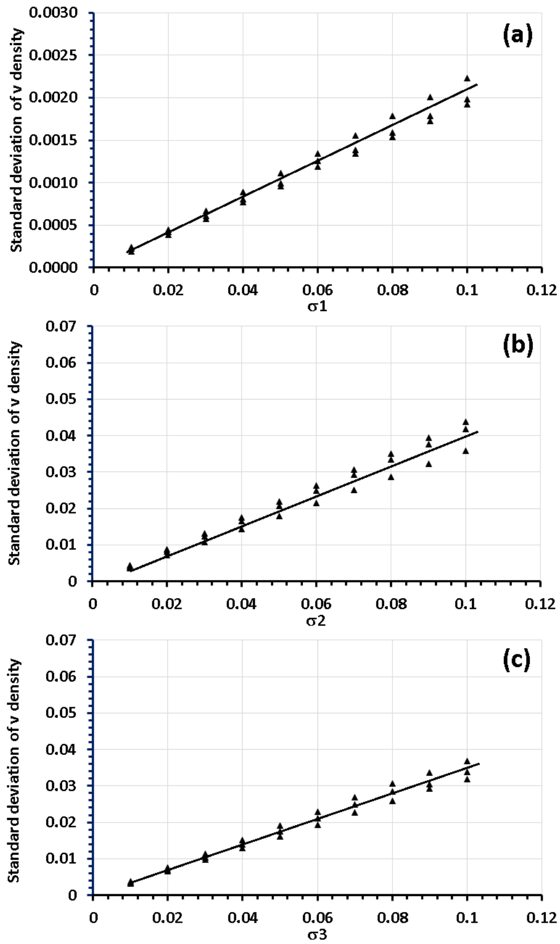

FIG. 4. Similar to Figure 3 but for the dependence of the standard deviation of TC intensity of the invariant intensity distribution ρ_Y as given by Eq. (11) of the stochastic TC-scale model on the individual standard deviation a) σ_1 assuming $\sigma_2 = \sigma_3 = 0$, b) σ_2 assuming $\sigma_1 = \sigma_3 = 0$, and c) σ_3 assuming $\sigma_1 = \sigma_2 = 0$.

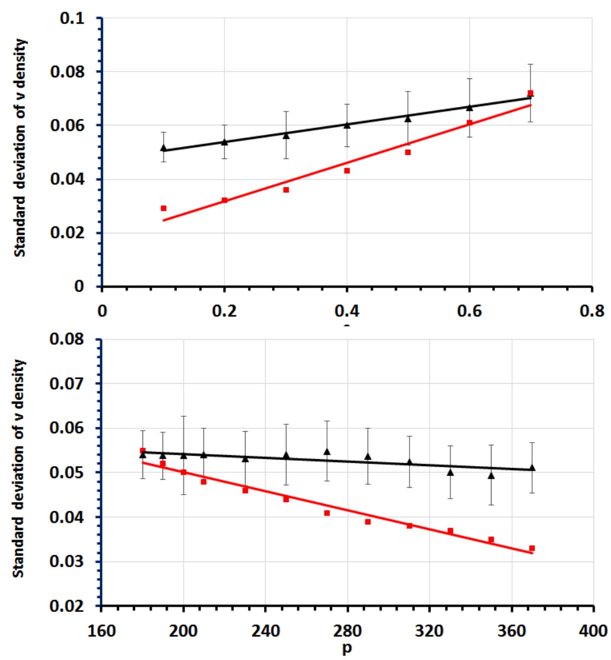

FIG. 5. Dependence of the standard deviation of TC intensity as obtained from the full nonlinear integration of Eq. (2) (black solid) and the approximated solution to the linearized system (red solid) on a) the model parameter p, and b) the model parameter s assuming $\sigma_1 = \sigma_2 = \sigma_3 = 0.1$.